Hindawi Publishing Corporation
Advances in Materials Science and Engineering
Volume 2013, Article ID 640428, 7 pages
http://dx.doi.org/10.1155/2013/640428

Research Article

A Humidity Sensor Based on Silver Nanoparticles Thin Film Prepared by Electrostatic Spray Deposition Process

Thutiyaporn Thiwawong,[1,2,3] Korakot Onlaor,[1,2,3] and Benchapol Tunhoo[1,2,3]

[1] *Electronics and Control System for Nanodevice Research Laboratory, College of Nanotechnology, King Mongkut's Institute of Technology Ladkrabang, Bangkok 10520, Thailand*
[2] *Thailand Center of Excellence in Physics, CHE, 328 Si Ayutthaya Road, Bangkok 10400, Thailand*
[3] *Nanotec-KMITL Excellence Center on Nanoelectronic Devices, Bangkok 10520, Thailand*

Correspondence should be addressed to Thutiyaporn Thiwawong; tthiwawong@gmail.com

Received 27 March 2013; Revised 10 May 2013; Accepted 19 May 2013

Academic Editor: Zhimin Liu

In this work, thin film of silver nanoparticles for humidity sensor application was deposited by electrostatic spray deposition technique. The influence of the deposition times on properties of films was studied. The crystal structures of sample films, their surface morphology, and optical properties have been investigated by X-ray diffraction (XRD), field emission scanning electron microscopy (FE-SEM), and UV-VIS spectrophotometer, respectively. The crystalline structure of silver nanoparticles thin film was found in the orientation of (100) and (200) planes of cubic structure at diffraction angles $2\theta = 38.2^{\circ}$ and 44.3°, respectively. Moreover, the silver nanoparticles thin films humidity sensor was fabricated onto the interdigitated electrodes. The sensor exhibited the humidity adsorption and desorption properties. The sensing mechanisms of the device were also elucidated by complex impedance analysis.

1. Introduction

The humidity measurement is essential in a wide range of industrial applications including the pharmaceutical, food, medicine, and electronics industries [1]. Some humidity sensors have been developed based on a reversible interaction between a material and water vapor, hence acting as a gas sensor [2]. Existing humidity sensing methodologies also rely upon optical, gravimetric, capacitive, resistive, piezoresistive, and magnetoelastic properties of selected materials [3]. Recently, it is reported that the use of nanostructures, such as nanoparticles, nanowire, nanotubes, and polymer nanocomposites, as the humidity sensing materials could enhance the performance of humidity sensors greatly [4–8]. For these nanostructured materials, the surface effect becomes dominant due to their large surface-to-volume ratio, which is beneficial to construct the humidity sensors and the gas sensors [9].

In the past few years, electrostatic spray deposition (ESD) technique has been used to prepare a variety of functional materials thin films. Compared with other film fabrication techniques, ESD is a simple set-up process, low cost, a wide choice of precursors, relatively large film growth rate, ambient atmosphere operation, and a good control of the morphology of the deposited layers. The ESD technique was used so far to deposit thin films of functional materials with application in different fields, that is, rechargeable lithium batteries [10], solid oxide fuel cells [11], heat exchange reactors [12], biomedical implants [13], and sensors [14, 15].

In this paper, we report the preparation of silver nanoparticles (Ag NPs) thin film by ESD technique. The structural, optical properties and surface morphology were investigated for using for the humidity sensor application. The sensing mechanism of the Ag NPs device was performed by the complex impedance analysis.

2. Experimental

For the deposition of the Ag NPs film a vertical ESD setup working under ambient atmosphere was used, as shown in Figure 1. The liquid precursor solution was fed by a syringe

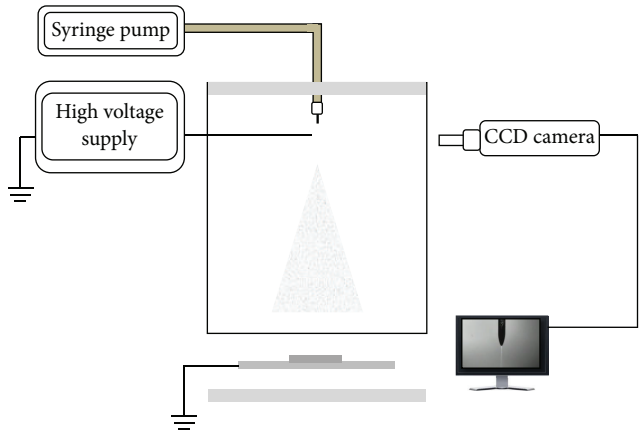

Figure 1: Electrostatic spray deposition experiment setup.

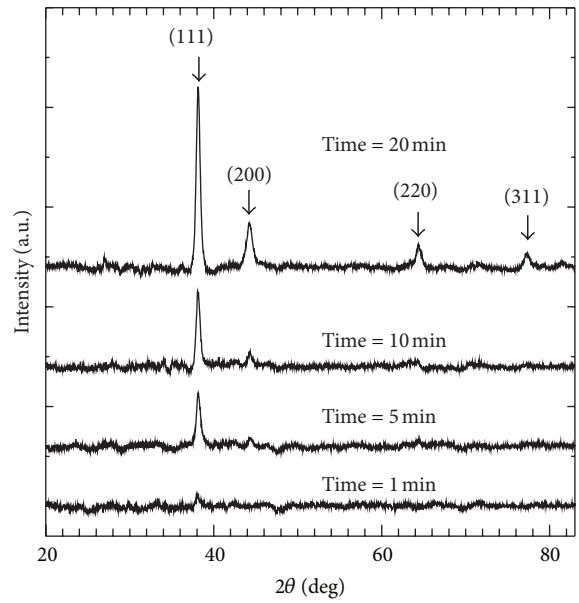

Figure 2: XRD patterns of Ag NPs film at various deposition times of 1, 5, 10, and 20 min.

pump through a plastic syringe to the tip of a stainless steel nozzle (inside diameter of 0.1 mm). When the high voltage is applied by a DC high voltage power supply between the nozzle and the substrate holder, the precursor solution is atomized at the tip of the nozzle into an aerosol of very fine droplets. This aerosol of highly charged droplets is directed to the substrate under the electrostatic force. When the droplets attached the substrate, the droplets are losing their charge and spreading; drying and decomposition of the precursor solution occur. In this way, a thin layer is formed on the substrate surface.

Silver nanoparticles solution (Aldrich, nanoparticles, <100 nm (TEM), 10 wt.% dispersion in ethylene glycol) was used as precursor solution. Glass substrate with dimension of 10 × 20 mm was cleaned by alcohol process and put onto an aluminum ground plate. ESD conditions were optimized by varying deposition time at 1, 5, 10, and 20 minute, respectively, while the nozzle to substrate distance was fixed at 40 mm. A 10 kV positive voltage was applied to the nozzle, breaking the liquid at the tip of the nozzle in an aerosol composed of very small droplets. Their crystal structures were analyzed by X-ray diffraction (Bruker). The morphology of thin films was studied by scanning electron microscope (S-4700, Hitachi). The optical absorption spectra have been characterized using UV-VIS spectrophotometer (HELIOS, Thermo Spectronic) The Ag NPs film was employed as the humidity sensitive material for sensor development. The sensor devices were fabricated by depositing the Ag NPs film onto the interdigitated electrode that was fabrication by print circuit board process. After that, the device was tested in the humidity-controlled measurement system. The humidity-controlled environments 11%, 23%, 32%, 52%, 75%, 84%, and 93% RH were achieved using saturated aqueous solution of LiCl, CH_3COOK, $MgCl_2$, $Mg(NO_3)_2$, NaCl, KCl, and KNO_3, respectively. A precision LCR meter (Agilent, E4980A) was used to measure the impedance characteristics during the humidity measurement. The AC impedance measurements were done in Z-θ_r mode for a frequency (f) of 1 kHz with an AC drive bias of 50 mV. The hysteresis characteristics were measured by first humidification process using fresh samples from 11% to 93% RH and directly return to the desiccation process from 93% to 11% RH. Response and recovery time was determined using the saturated salt solution of KNO_3 for 93% RH and LiCl for 11% RH. The response time from 11% to 93% RH was measured by quickly transferring the humidity sensor from the chamber in equilibrium at 11% RH to the chamber in equilibrium at 93% RH.

3. Results and Discussion

XRD spectra of the Ag NPs film at a fixed nozzle to substrate distances of 40 mm for various the deposition times are shown in Figure 2. XRD pattern exhibits a polycrystalline nature, with the diffraction peaks indexed and compared with standard data in the JCPDS-ICDD. The dominant peaks were observed at $2\theta = 38.2^\circ$ and the subtle peak at $2\theta = 44.3^\circ$, which correspond to the (111) and (200) planes of cubic structure respectively. The intensity of peaks increases with increasing deposition time, whereas the full width at the half-maximum (FWHM) decrease with increasing deposition time. The decrease in FWHM can be explained by the decrease in the concentration of lattice imperfections, due to the decrease in the internal microstrain with in the films, and an increase in the crystalline size.

The crystalline size (D) was calculated using the Scherrer equation [16]

$$D = \frac{k\lambda}{\beta \cos\theta}, \quad (1)$$

where β is FWHM, k is constant (with a value of 0.94), λ is wavelength of the X-ray radiation and is the Bragg angle. The dislocation density (δ) and is defined as the length of

Table 1: Structural parameters (crystalline size, dislocation density, and lattice microstrain) of the Ag NPs film deposited at different deposition times.

Deposition time	D (nm)	δ (10^{14} lin m^{-2})	ε (10^{-3} lin^{-2} m^{-2})
5 min	14.8	45.1	1.89
10 min	16.5	36.3	1.71
20 min	17.1	34.2	1.65

dislocation lines per unit value of crystal, that was evaluated using Williamson and Smallman's formula [16]

$$\delta = \frac{1}{D^2}. \tag{2}$$

The strain function (ε) in the films was calculated using the relation [16]

$$\varepsilon = \left(\frac{\lambda}{D\cos\theta} - \beta\right)\left(\frac{1}{\tan\theta}\right). \tag{3}$$

From Table 1, the crystalline size from XRD was observed to increase, while the dislocation density and the strain decreased with increasing deposition time. Typically, stress also occurs in the film due to the lattice misfit. Nevertheless, the stress has two components: thermal stress arising from the difference in the expansion coefficient of the film and substrate, and internal stress due to the accumulating effect of the crystallographic flaws built into the films during deposition. The average stress of the deposited films was found to be compression in nature. This compressive stress is due to the grain boundary effect, which is predominant in polycrystalline films [16].

Figure 3 depicts the surface morphology of Ag NPs film at various deposition thin films. The Ag NPs film prepared at deposition time of 1 min is found to consist of small grains, as shown in Figure 3(a). When the deposition time is increased, the surface coverage increases because the cluster of Ag NPs will pile up on substrate as shown in Figures 3(b) and 3(d). At an increased deposition time, the large grains were observed. The formation of the dense layer morphology was a clear indication that the solvent in the spray droplets has not been evaporated completely when arriving at the substrate surface. The droplet solution might have spread on the substrate surface and formed a continuous layer. Usually, on a substrate, the spreading rate is larger than on the thin film layer. Therefore, droplets were well spread on the substrate. For shorter deposition time, small grains layers were generated. This effect can be explained by the complete evaporation of liquid droplets. On the other hand, with a longer the deposition time, the continuous layers were observed. This generation was attributed to the layer formed by the incompletely evaporated droplets [17].

The room temperature optical absorption spectra of Ag NPs film at various deposition times in the wavelength region 300–900 nm are shown in Figure 4. In this spectral performed, the main absorption peak was observed at around 440 nm corresponding to a peculiar characteristic of the silver nanoparticles surface plasmon. It is found that the main absorption peak was slightly red shifted when the deposition time is increased. This result agrees well with the Mie theory for the surface plasmon peak of nanoparticles in UV-visible absorption spectra. According to the Mie theory, silver nanoparticles of diameters ranging from 1 to 10 nm have the plasmon peak width increasing linearly with the reciprocal of the particle diameter [18, 19]. The surface plasmon peak of a larger nanoparticle is more narrowed (intrinsic size effect) [20]. However, when the particle diameter increases further (>20 nm) the peak width increases with the particle diameter (extrinsic size effect).

To investigate the humidity sensing properties of Ag NPs film, the humidity sensor device has been fabricated by deposited Ag NPs film on the interdigitated electrodes at nozzle to substrate distance of 40 mm with various deposition times of 1, 5, 10, and 20 min, respectively. When the humidity environment changes, the moisture was absorbed by the Ag NPs film and lead to the change of device impedance characteristics. With the relative humidity increasing, the impedance of Ag NPs sensor shifted to the lower impedance monotonically. The relationships between the shifted impedance for Ag NPs sensor and the relative humidity are shown in Figure 5. The tested humidity levels ranged from 11% RH to 93% RH. The sensitivity of the device that depends on the cluster of Ag NPs film can be described below. While the Ag NPs films were prepared at low deposition times, the surface morphology of films exhibited the small grain of Ag NPs cluster, whereas at the condition of high deposition times, the large continuous grain of Ag NPs clusters was observed. Typically, the grain boundary effect has been dominated to the carriers transport in the films; therefore, the device that prepared at high deposition time will show the high sensitivity.

To study the repeatability properties, the sensors were tested in two fixed humidity levels repeatedly and the continuous impedance values were records. The sensor responses under two humidity conditions that corresponded to 11%–93%–11% RH, respectively, were tested and the results are shown in Figure 6. It is found that the magnitude of the responds between the two states of % RH is about 10^3 values. The time constants for absorption and desorption of the Ag NPs sensor can be evaluated form the graph with the values about 4 and 2 second, respectively. When the relative humidity is increased, the device impedance decreases due to the effect of water moisture in the Ag NP sensing layer. Normally at the higher relative humidity levels, the ion of water moisture can be captured with the silver nanoparticles network and the mobility of electron in Ag NPs film has been increased; therefore the impedance of the device was decreased [21]. More details of sensing mechanism were discussed later.

The hysteresis curve is shown in Figure 7. From the hysteresis error formula $\gamma_H = \pm(1/2)(\Delta H_{\max}/F_{\mathrm{FS}})$, where $\Delta H_{\max}$ is the maximum differences output in forward and backward operations and F_{FS} is the full scale output, the hysteresis of the humidity sensors at the prepared conditions

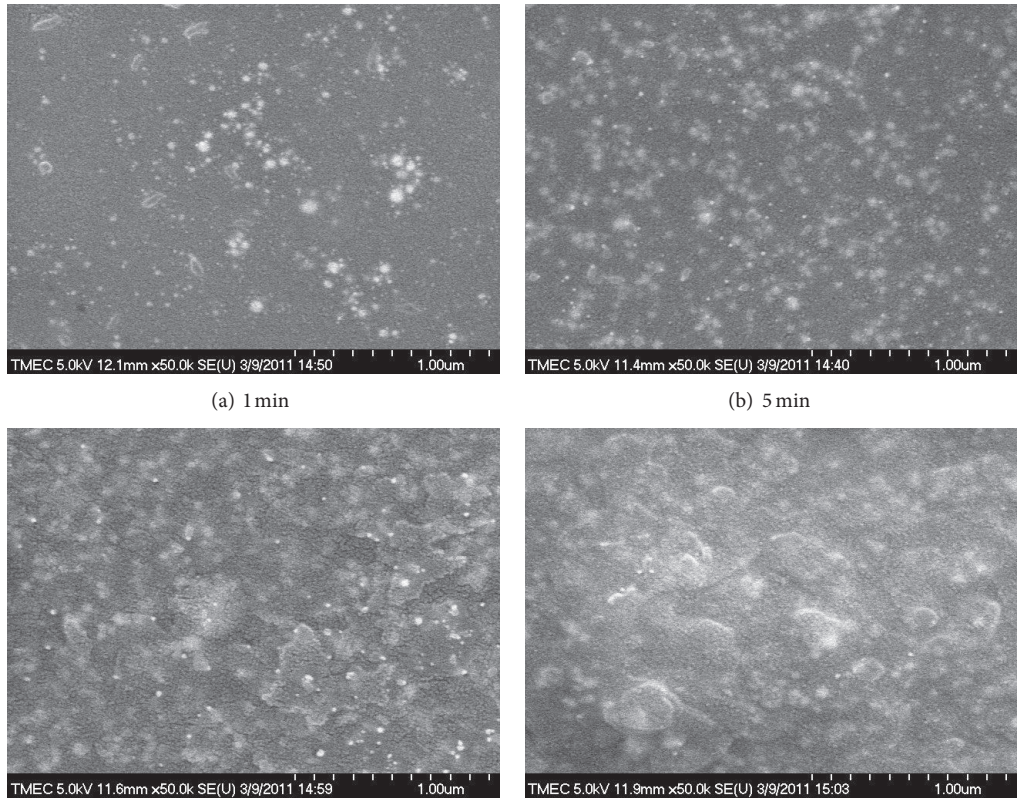

(a) 1 min (b) 5 min

(c) 10 min (d) 20 min

Figure 3: SEM images of Ag NPs film at various deposition times of (a) 1 min, (b) 5 min, (c) 10 min, and (d) 20 min.

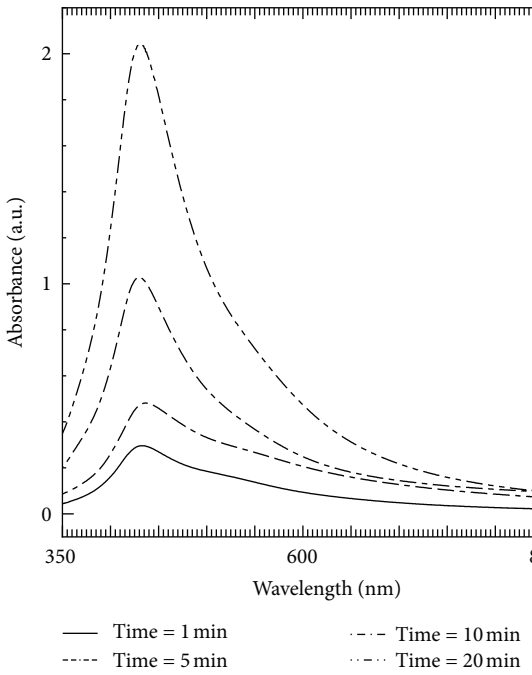

Figure 4: Optical absorption spectra of Ag NPs film at various deposition times of 1, 5, 10, and 20 min.

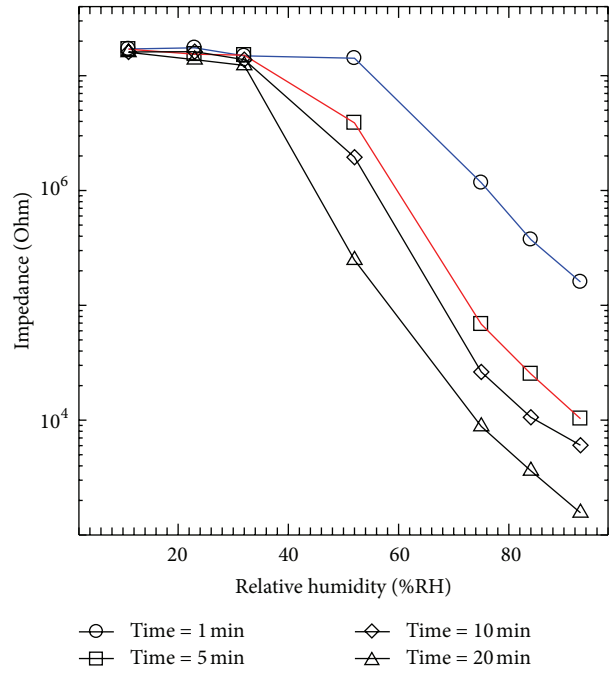

Figure 5: The relationships between the impedance of Ag NPs humidity sensor and the relative humidity.

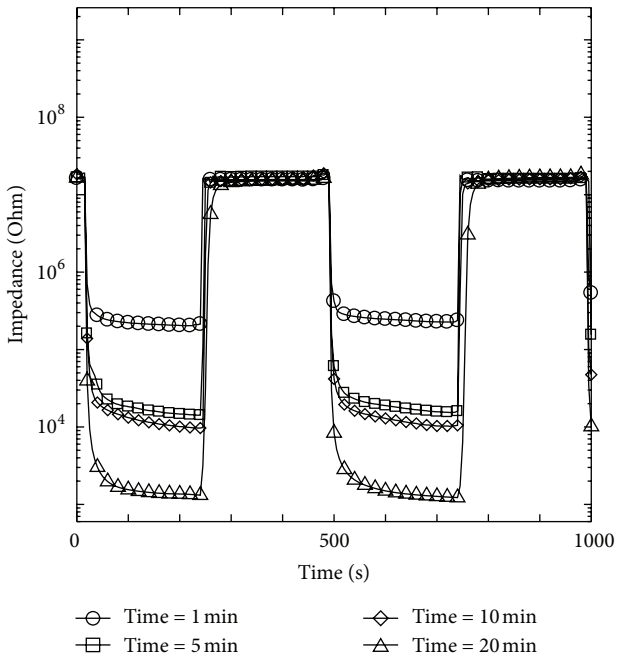

Figure 6: Response time of the Ag NPs humidity sensor at different deposition time under humidity cycling of 11%–93%–11% RH.

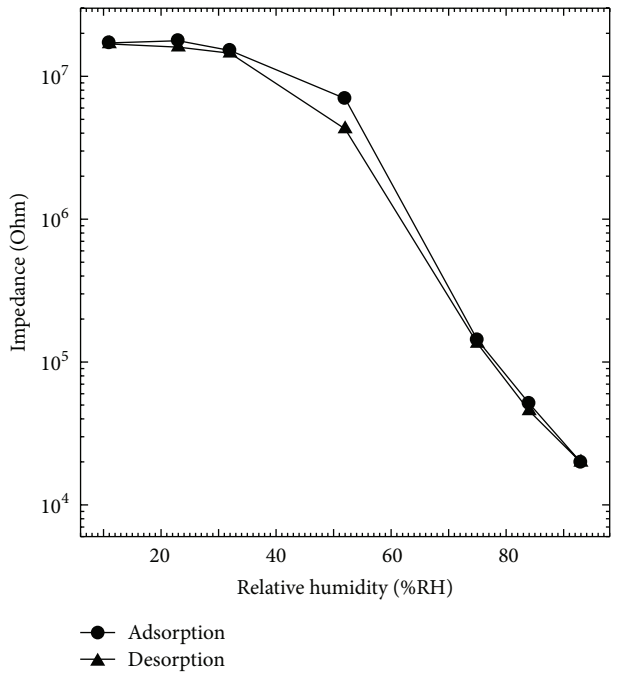

Figure 7: Hysteresis characteristics of the Ag NPs humidity sensor at deposition time of 5 min.

of deposition distance and time were 40 mm and 5 min, was also investigated. The maximum absolute value of humidity hysteresis error (γ_H) was ±7.8% corresponding to 52% RH.

The stability of the sensor of the device with deposition time of 5 min has been observed by repeat impedance measurement over a period of 15 days at various humidity

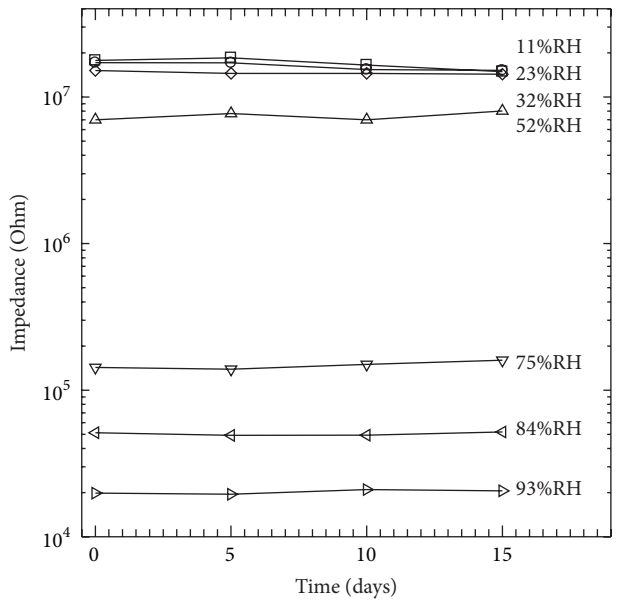

Figure 8: Stability of the Ag NPs humidity sensor at deposition times of 5 min after being kept at the ambient condition.

levels. The stability curve is shown in Figure 8. That can be seen that the stability of Ag NP humidity is also quite stable in 15 days. Experiments carried out with freshly deposited devices were found to be not different from the stored devices. The maximum change from the origin value after 15 days is 16.1% at 23% RH.

The sensing mechanisms of the Ag NPs humidity sensor were investigated through the analysis of complex impedance plot. The complex ac impedance measurements were done in Z-θ_r mode for a varying frequency (f), from 20 Hz to 1 MHz with an AC drive bias of 50 mV and DC bias of 0 V. Cole-cole plots of the measurements are depicted in Figure 9. At low relative humidity region, the cole-cole plot exhibited the semicircular patterns. A semicircle Nyquist diagram indicates that the sensor could be described by the Randles equivalent circuit as shown in Figure 10(a). In the RC circuit, R_S corresponds to the series resistance; R_P and C_P are the resistance and capacitance of the device. R_P is corresponding to the real impedance of Ag nanoparticles film and C_P can be achieved from the imaginary impedance part. This semicircular Nyquist diagram indicates that the sensor operates through a hopping mechanism which the discrete jump of the charge carriers from one site to another over energy barriers. Under this condition, no continuous aquatic layer is formed owing to the insufficient adsorption of water vapor [22–25].

In case of high relative humidity region, a linear tail occurred at lower frequencies accompanied by a significant decrease of the semicircular part. The Warburg impedance (Z_w) element was added in series with R_P to the equivalent circuit as shown in Figure 10(b), which represents the involvement of diffusion of reactants [26]. If the adsorption is increased further the resulting Nyquist diagram is

a 45° line for all frequencies. Here, the electrolytic condition mainly arises from the faster diffusion of protons in single or multilayers that are formed on the material surface [27, 28]. This facilitates carrier transportation and favors polarization as well, thereby allowing for a large impedance response. The transition threshold of the two sensing mechanisms for the Ag nanoparticles sensor is about 32%–52% RH at room temperature as shown in Figures 5 and 9. To investigate the effect of moisture absorption to the structure of Ag NPs film, the energy-dispersive X-ray spectroscopy (EDS) and Raman spectroscopy measurements were used to analyze the composition of Ag NPs film before and after humidity cycling as shown in the supplementary figures shown in Supplementary Material available online at http://dx.doi.org/10.1155/2013/640428. The supplementary materials exhibited the EDS spectra and Raman spectra of Ag NPs films before and after humidity cycling. Found that the amount of compositions in EDS spectra of Ag NPs film that are shown slightly fluctuation at after humidity cycling, which is consistent with the result of Raman spectroscopy. It has been reported about the phase transformations of Ag NPs due to the environmental conditions such as UV-light and water droplet [29–31], but usually in the form of a solution, which is a condition that depends on factors of thermodynamic. However, in this work, Ag NPs films are used as the sensing layer, exposed to moisture vapor at the surface. Thus, it is possible to change on the surface structure and surface properties of the sensor, while the sensing region of device will be occurred at the surface region of films that corresponding to the impedance measurement, which was mentioned previously.

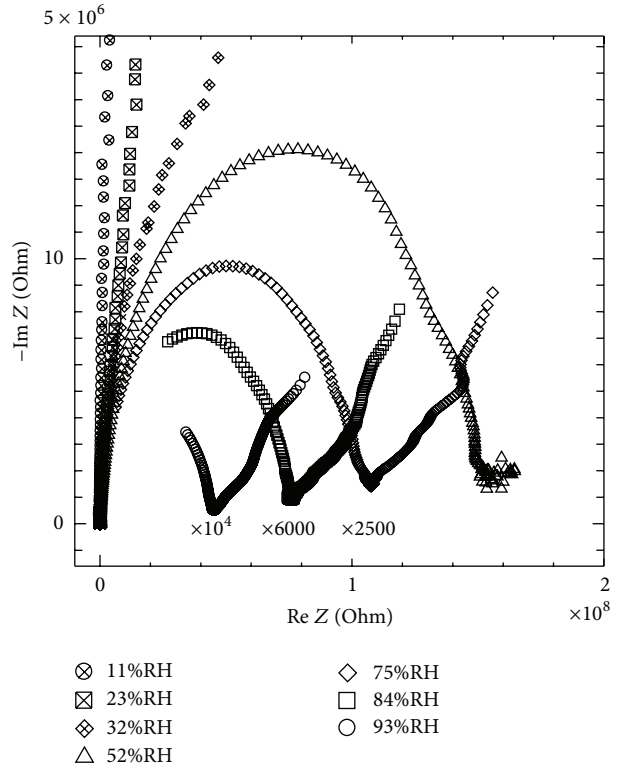

Figure 9: Complex impedance plot of Ag NPs humidity sensor at deposition time of 5 min for different relative humidities at room temperature.

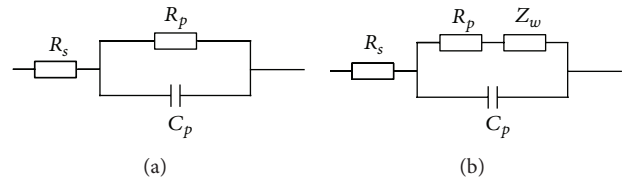

Figure 10: The equivalent circuit of sensors showing (a) a hopping mechanism and (b) an ion diffusion mechanism.

4. Conclusion

The thin films of silver nanoparticles for humidity sensor applications have been deposited by electrostatic spray deposition technique. The effect of the deposition time on the properties of films was investigated. The crystal structure of silver nanoparticle thin films was founded in the orientation of (100) and (200) planes of cubic structure at diffraction angles $2\theta = 38.2^\circ$ and 44.3°, respectively. The optical absorption peak was observed at around 440 nm, which is the surface plasmon peak of nanoparticles in UV-visible absorption spectra. The surface morphology of Ag NPs film also depended on the deposition time. Moreover, the silver nanoparticles thin film humidity sensor was fabricated onto the interdigitated electrodes. The sensor exhibits the humidity adsorption and desorption properties with the responsibility in ranges of 11% RH to 93% RH. The time constants for absorption and desorption of the Ag NPs sensor can be evaluated from the cycling measurement with the values about 4 and 2 second, respectively. The maximum hysteresis was found at ±7.8% of full scale output at 52% RH. In addition, the long-term stability of the silver nanoparticles humidity sensor can be demonstrated by keep the device at the ambient condition without encapsulation with 15 days. By complex impedance analysis, the sensing mechanisms could be ascribed to the hopping charge transfer at low relative humidity region and the charge diffusion mechanism at high relative humidity region.

Acknowledgment

This work has partially been supported by the National Nanotechnology Center (NANOTEC), NSTDA, Ministry of Science and Technology, Thailand, through its program of Center of Excellence Network and the National Research Council of Thailand.

References

[1] P. K. Kannan, R. Saraswathi, and J. B. B. Rayappan, "A highly sensitive humidity sensor based on DC reactive magnetron sputtered zinc oxide thin film," *Sensors and Actuators A*, vol. 164, no. 1-2, pp. 8–14, 2010.

[2] A. C. Power, A. J. Betts, and J. F. Cassidy, "Silver nanoparticle polymer composite based humidity sensor," *Analyst*, vol. 135, no. 7, pp. 1645–1652, 2010.

[3] C. Lee and G. Lee, "Humidity sensors: a review," *Sensor Letters*, vol. 3, no. 1, pp. 1–15, 2005.

[4] M. V. Fuke, A. Vijayan, P. Kanitkar, and R. C. Aiyer, "Optical humidity sensing characteristics of Ag-polyaniline nanocomposite," *IEEE Sensors Journal*, vol. 9, no. 6, pp. 648–653, 2009.

[5] C. Baratto, E. Comini, G. Faglia, G. Sberveglieri, M. Zha, and A. Zappettini, "Metal oxide nanocrystals for gas sensing," *Sensors and Actuators B*, vol. 109, no. 1, pp. 2–6, 2005.

[6] P. L. P. Hoa, G. Suchaneck, and G. Gerlach, "Influence of polycrystalline silicon as electrical shield on reliability and stability of piezoresistive sensors," *Sensors and Actuators A*, vol. 120, no. 2, pp. 567–572, 2005.

[7] Y. Sakai, Y. Sadaoka, and M. Matsuguchi, "Humidity sensors based on polymer thin films," *Sensors and Actuators B*, vol. 35, no. 1–3, pp. 85–90, 1996.

[8] X. H. Wang, Y. F. Ding, J. Zhang et al., "Humidity sensitive properties of ZnO nanotetrapods investigated by a quartz crystal microbalance," *Sensors and Actuators B*, vol. 115, no. 1, pp. 421–427, 2006.

[9] B. Tao, J. Zhang, F. Miao, H. Li, L. Wan, and Y. Wang, "Capacitive humidity sensors based on Ni/SiNWs nanocomposites," *Sensors and Actuators B*, vol. 136, no. 1, pp. 144–150, 2009.

[10] C. H. Chen, A. A. J. Buysman, E. M. Kelder, and J. Schoonman, "Fabrication of $LiCoO_2$ thin film cathodes for rechargeable lithium battery by electrostatic spray pyrolysis," *Solid State Ionics*, vol. 80, no. 1-2, pp. 1–4, 1995.

[11] O. Wilhelm, S. E. Pratsinis, D. Perednis, and L. J. Gauckler, "Electrospray and pressurized spray deposition of yttria-stabilized zirconia films," *Thin Solid Films*, vol. 479, no. 1-2, pp. 121–129, 2005.

[12] M. Nomura, B. Meester, J. Schoonman, F. Kapteijn, and J. A. Moulijn, "Preparation of thin porous titania films on stainless steel substrates for heat exchange (HEX) reactors," *Separation and Purification Technology*, vol. 32, no. 1–3, pp. 387–395, 2003.

[13] S. C. G. Leeuwenburgh, J. G. C. Wolke, J. Schoonman, and J. A. Jansen, "Deposition of calcium phosphate coatings with defined chemical properties using the electrostatic spray deposition technique," *Journal of the European Ceramic Society*, vol. 26, no. 4-5, pp. 487–493, 2006.

[14] E. H. A. Diagne and M. Lumbreras, "Elaboration and characterization of tin oxide-lanthanum oxide mixed layers prepared by the electrostatic spray pyrolysis technique," *Sensors and Actuators B*, vol. 78, no. 1–3, pp. 98–105, 2001.

[15] H. Gourari, M. Lumbreras, R. van Landschoot, and J. Schoonman, "Electrode nature effects on stannic oxide type layers prepared by electrostatic spray deposition," *Sensors and Actuators B*, vol. 58, no. 1–3, pp. 365–369, 1999.

[16] K. Onlaor, B. Tunhoo, P. Keeratithiwakorn, T. Thiwawong, and J. Nukeaw, "Electrical bistable properties of copper phthalocyanine at different deposition rates," *Solid-State Electronics*, vol. 72, pp. 60–66, 2012.

[17] J. Jeong, Y. Jeon, K. Jeon, K. Hwang, and B. Kim, "Preparation of zinc oxide films by an electrostatic spray deposition process," *Journal of Ceramic Processing Research*, vol. 7, no. 1, pp. 70–74, 2006.

[18] F. Mafuné, J. Kohno, Y. Takeda, T. Kondow, and H. Sawabe, "Structure and stability of silver nanoparticles in aqueous solution produced by laser ablation," *Journal of Physical Chemistry B*, vol. 104, no. 35, pp. 8333–8337, 2000.

[19] C. Petit, P. Lixon, and M. Pileni, "In situ synthesis of silver nanocluster in AOT reverse micelles," *Journal of Physical Chemistry*, vol. 97, no. 49, pp. 12974–12983, 1993.

[20] U. Kreibig and M. Vollmer, *Optical Properties of Metal Clusters*, Springer, Berlin, Germany, 1995.

[21] Z. Chen and C. Lu, "Humidity sensors: a review of materials and mechanisms," *Sensor Letters*, vol. 3, no. 4, pp. 274–295, 2005.

[22] L. Gu, K. Zheng, Y. Zhou et al., "Humidity sensors based on ZnO/TiO_2 core/shell nanorod arrays with enhanced sensitivity," *Sensors and Actuators B*, vol. 159, no. 1, pp. 1–7, 2011.

[23] K. Ogura, T. Tonosaki, and H. Shiigi, "AC impedance spectroscopy of humidity sensor using poly(o-phenylenediamine)/poly(vinyl alcohol) composite film," *Journal of the Electrochemical Society*, vol. 148, no. 3, pp. H21–H27, 2001.

[24] Y. Li, M. J. Yang, and Y. She, "Humidity sensors using in situ synthesized sodium polystyrenesulfonate/ZnO nanocomposites," *Talanta*, vol. 62, no. 4, pp. 707–712, 2004.

[25] E. Traversa, A. Bearzotti, M. Miyayama, and H. Yanagida, "Study of the conduction mechanism of La_2CuO_4–ZnO heterocontacts at different relative humidities," *Sensors and Actuators B*, vol. 25, no. 1–3, pp. 714–718, 1995.

[26] M. Vrňata, D. Kopecký, F. Vysloužil et al., "Impedance properties of polypyrrolic sensors prepared by MAPLE technology," *Sensors and Actuators B*, vol. 137, no. 1, pp. 88–93, 2009.

[27] C. D. Feng, S. L. Sun, H. Wang, C. U. Segre, and J. R. Stetter, "Humidity sensing properties of Nafion and sol-gel derived SiO_2/Nafion composite thin films," *Sensors and Actuators B*, vol. 40, no. 2-3, pp. 217–222, 1997.

[28] J. Wang, Q. H. Lin, R. Zhou, and B. K. Xu, "Humidity sensors based on composite material of nano-$BaTiO_3$ and polymer RMX," *Sensors and Actuators B*, vol. 81, no. 2-3, pp. 248–253, 2002.

[29] J. M. Gorham, R. I. MacCuspie, K. L. Klein, D. H. Fairbrother, and R. D. Holbrook, "UV-induced photochemical transformations of citrate-capped silver nanoparticle suspensions," *Journal of Nanoparticle Research*, vol. 14, article 1139, 2012.

[30] X. Jiang, X. Zhou, Y. Zhang, T. Zhang, Z. Guo, and N. Gu, "Interfacial effects of in situ-synthesized ag nanoparticles on breath figures," *Langmuir*, vol. 26, no. 4, pp. 2477–2483, 2010.

[31] C. Levard, E. M. Hotze, G. V. Lowry, and G. E. Brown, "Environmental transformations of silver nanoparticles: impact on stability and toxicity," *Environmental Science and Technology*, vol. 46, no. 13, pp. 6900–6914, 2012.